JOURNAL OF GEOPHYSICAL RESEARCH, VOL. 114, E05001, doi:10.1029/2008JE003286, 2009

Constraints on deep moonquake focal mechanisms through analyses of tidal stress

R. C. Weber,[1] B. G. Bills,[2,3] and C. L. Johnson[2,4]

Received 24 October 2008; revised 12 February 2009; accepted 5 March 2009; published 12 May 2009.

[1] A relationship between deep moonquake occurrence and tidal forcing is suggested by the monthly periodicities observed in the occurrence times of events recorded by the Apollo Passive Seismic Experiment. In addition, the typically large S wave to P wave arrival amplitude ratios observed on deep moonquake seismograms are indicative of shear failure. Tidal stress, induced in the lunar interior by the gravitational influence of the Earth, may influence moonquake activity. We investigate the relationship between tidal stress and deep moonquake occurrence by searching for a linear combination of the normal and shear components of tidal stress that best approximates a constant value when evaluated at the times of moonquakes from 39 different moonquake clusters. We perform a grid search at each cluster location, computing the stresses resolved onto a suite of possible failure planes, to obtain the best fitting fault orientation at each location. We find that while linear combinations of stresses (and in some cases stress rates) can fit moonquake occurrence at many clusters quite well; for other clusters, the fit is not strongly dependent on plane orientation. This suggests that deep moonquakes may occur in response to factors other than, or in addition to, tidal stress. Several of our inferences support the hypothesis that deep moonquakes might be related to transformational faulting, in which shear failure is induced by mineral phase changes at depth. The occurrence of this process would have important implications for the lunar interior.

Citation: Weber, R. C., B. G. Bills, and C. L. Johnson (2009), Constraints on deep moonquake focal mechanisms through analyses of tidal stress, *J. Geophys. Res.*, *114*, E05001, doi:10.1029/2008JE003286.

1. Introduction

[2] The Apollo Passive Seismic Experiment [*Latham et al.*, 1969] consisted of a network of four seismometers deployed on the lunar surface between 1969 and 1972 that recorded continuously until 1977. Many types of seismic events were detected by these instruments, including surface impacts of natural and man-made objects, shallow moonquakes of thermal and possibly tectonic origin, and deep moonquakes, widely assumed to be associated with the lunar tides. Deep moonquakes are the most common event type detected by the experiment, comprising approximately half of the event catalog [*Nakamura et al.*, 1981]. They occur in localized regions, often referred to as "clusters," which are located mostly on the lunar nearside at depths between approximately 550 and 1420 km (Figure 1) [*Nakamura*, 2005]. Each cluster exhibits its own characteristic, repeatable waveform, and produces events at 27- to 29-day intervals, reflecting the dynamics of the Earth-Moon system. Some clusters produce one event per month, with long periods of inactivity (sometimes up to several months); other clusters produce multiple events per month, with the largest event typically followed by one or more smaller events in short succession (within days). Despite these differences in detailed behavior, almost all clusters exhibit some level of tidal periodicity [*Ewing et al.*, 1971; *Bulow*, 2007].

1.1. Our Goal

[3] We are interested in determining whether deep moonquake occurrence is related in a predictable way to tidal stress, which likewise varies periodically owing to the effect of Earth's gravitational influence on the Moon. Specifically, we test whether deep moonquakes can be explained using a mechanism similar to the Coulomb stress criterion [see, e.g., *Pollard and Fletcher*, 2005], in which shear failure occurs at some critical value of shear and normal tidal stress, as resolved on a planar fault surface at depth. If a planar fault surface is identified, we report the parameters describing this plane: the fault dip and strike. These parameters partially describe the focal mechanism, which consists of fault dip, strike, and rake [*Aki and Richards*, 2002].

[4] Our proposed moonquake failure mechanism is motivated by a criterion formulated for terrestrial seismology. The Coulomb stress criterion has been used to show that stress accumulation rate is related to earthquake recurrence intervals [*Smith and Sandwell*, 2003]. Over a characteristic time, tectonic stress accumulates and is intermittently released.

[1] U.S. Geological Survey, Flagstaff, Arizona, USA.
[2] Cecil H. and Ida M. Green Institute of Geophysics and Planetary Physics, Scripps Institution of Oceanography, University of California, San Diego, La Jolla, California, USA.
[3] NASA Jet Propulsion Laboratory, Pasadena, California, USA.
[4] Department of Earth and Ocean Sciences, University of British Columbia, Vancouver, British Columbia, Canada.

0148-0227/09/2008JE003286$09.00

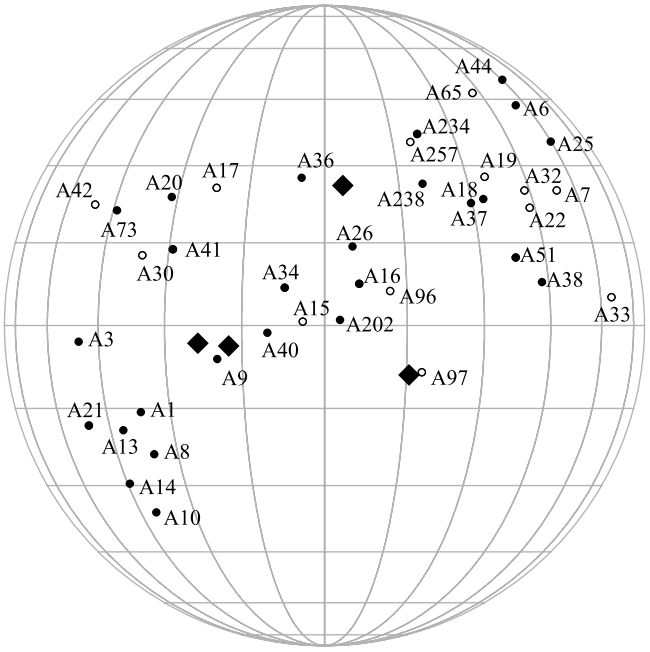

Figure 1. Map of the nearside of the Moon showing the 39 clusters (circles) analyzed in this study. All but one of these (A14) represent located clusters [*Nakamura*, 2005] with errors in latitude and longitude $\leq 10^\circ$ that include at least 35 events in the latest catalog [*Nakamura et al.*, 1981]. The depths of these 39 clusters range from 747 to 1343 km. Note A33 is a farside cluster; its longitude has been projected onto the nearside for plotting. The seismic stations (diamonds) are, from the west, Apollo 12, 14, 15, and 16. Open circles mark the 13 clusters with well-constrained fault plane orientations (see section 4).

If we extend this analogy to deep moonquakes, substituting a periodically varying tidal stress for a constant tectonic stress rate, then deep moonquakes may occur at a preferred stress state each tidal cycle. Two characteristics of deep moonquakes support this hypothesis: first, their tidal periodicity (mentioned above), and second, the likely double-couple nature of their focal mechanisms. Deep moonquake seismograms exhibit clearly defined compression (P) and shear (S) arrivals, with typically large S to P amplitude ratios. In addition, deep moonquake signal spectra are typically flat. These observations are consistent with shear failure on a plane [*Lammlein et al.*, 1974].

[5] In addition to testing the relationship between deep moonquake occurrence and (shear and normal) tidal stress, we also test whether deep moonquakes are sensitive to the rates of change of shear and normal tidal stress. This test is motivated by the results of *Bills et al.* [2008] and *Bulow* [2007], who found that moonquake times at some clusters correspond strongly to the rate of change of the orbital parameters describing the position of the Earth relative to the Moon. Since these parameters are likewise used to formulate the tidal stress, it is possible that deep moonquake occurrence times are also related in some way to stress rates.

1.2. Previous Work

[6] The possible relationship between moonquakes and tidal stress was suggested early in the Apollo experiment [*Latham et al.*, 1971], and we are not the first group to explore this relationship. However, because neither the fault plane orientation nor the friction coefficient at depth (both of which are needed to formulate the Coulomb stress) were known, earlier works applied various alternative methods in order to understand the physical process behind deep moonquakes. We now review these works.

1.2.1. Tidal Stress Analyses

[7] Stress is expressed in 3×3 tensor form, where each component of the tensor represents the traction on the plane formed by the two corresponding coordinate axes. The maximum tidal shear stress (defined as the difference between the maximum and minimum principal stresses) for a layered, elastic model of the Moon (having a decreased rigidity below 500 km depth) was found to reach a broad peak in the active source region, between approximately 600 and 1000 km depth. The coincidence of the deep moonquake source region with this broad stress peak supports the idea that deep moonquake occurrence is related to tidally induced shear failure [*Toksöz et al.*, 1977; *Cheng and Toksöz*, 1978].

[8] Some aspects of the tidal stress tensor (when computed using the locations of deep moonquake clusters) have been evaluated with respect to event occurrence times. *Toksöz et al.* [1977] found that the maxima of certain stress tensor components coincide with moonquake times at the A1 and A18 clusters. *Minshull and Goulty* [1988] also found A1 occurrence times to correlate with peaks of certain tidal stress tensor components, but only over short periods of time, and not consistently over the course of the whole experiment. *Lammlein* [1977] investigated several moonquake clusters and suggested that events occurred near extrema of the principal tidal shear stress, or during periods of increasing stress. *Goulty* [1979] tested a Coulomb criterion against deep moonquake occurrence at A1 by assuming a range of values for the friction factor and resolving the stress tensor onto a coarse grid of fault parameters, but did not find a good correlation.

1.2.2. Attempts at Focal Mechanism Recovery

[9] Various characteristics of deep moonquake seismograms make them unsuitable for application of typical terrestrial focal mechanism recovery methods, which require observations of first-motion polarities at a large number of seismic stations covering a large geographical area with respect to the epicenter. The lunar seismic data are limited by both the small number and the ~1300 km spacing of the stations, in addition to scattering of seismic energy by the fractured regolith, which precludes the identification of first-motion polarity [*Nakamura*, 1978]. Previous attempts at focal mechanism recovery therefore developed different methods to analyze deep moonquake focal mechanisms.

[10] Two studies presented failure plane orientations based on tidal stress analyses. *Toksöz et al.* [1977] suggested that moonquake activity coincided with minimum compression and maximum shear stress on a plane perpendicular to the Earth-Moon axis. *Lammlein* [1977] observed, among clusters associated with hypothetical moonquake "belts," that the largest deep moonquakes usually occur near alignments of the tidal shear stress corresponding to thrust faulting on planes parallel to each belt and dipping 30° to 40° from horizontal.

[11] *Araki* [2001] searched for failure planes such that moonquake times were coincident with monthly peaks in the shear stress, at several different moonquake locations. However, rather than reporting the best fitting planes, the degree to which events times were found to coincide with stress peaks was used to classify clusters as either tidally driven (caused entirely by tidal stress) or tidally triggered (caused by nontidal internal stress).

[12] Last, two additional studies estimated focal mechanisms from waveform properties. *Nakamura* [1978] analyzed the P wave to S wave arrival amplitude ratios for individual A1 moonquakes, and concluded that the moonquakes likely occurred on a locally horizontal plane, with varying slip directions. *Koyama and Nakamura* [1980] found some focal mechanisms consistent with this idea, on the basis of analyses of the S wave polarization of individual events.

1.2.3. Stress Rate Analyses

[13] The dependence of deep moonquake occurrence on stress rates has not been investigated previously. *Goulty* [1979] suggested that, in the presence of some slowly varying tectonic stress, moonquake activity might be expected when successive monthly tidal stress peaks reached amplitudes not attained for many months previously. *Minshull and Goulty* [1988] observed similar behavior for A1 events. An alternative interpretation of the coincidence of moonquake times with monthly stress peaks is that some moonquake clusters are sensitive to stress rates, since the stress rate is a constant (zero) at the times of stress extrema and hence could be included in a threshold-type failure criterion. No previous study has attempted to link moonquake occurrence to the rate of change of tidal stresses in such a manner.

1.3. Motivation for Our Work

[14] Although several studies have investigated both the influence of tidal stress on deep moonquake occurrence and deep moonquake focal mechanisms, no clear understanding of the physical process behind these events has emerged. The aforementioned works largely provide differing or contradictory results. This could be due to several factors, which we now review, followed by a description of how our work will address the problem.

1.3.1. Possible Complications in Stress Studies

[15] In computing the tidal stress, the choice of coordinate system varies from study to study. Likewise in examining the tidal stress at moonquake times, different studies use different parts of the stress tensor: some examine individual terms of the stress tensor; some resolve the stress tensor into its shear and normal components. These circumstances complicate comparisons among studies. In one extreme case, *Minshull and Goulty* [1988] were unable to reproduce the results of *Cheng and Toksöz* [1978], owing to the complicated coordinate system adopted in the latter.

[16] All of the previous studies mentioned in section 1.2 used early versions of the event catalog [*Nakamura et al.*, 1981], and usually focused on only the largest-amplitude monthly event when examining the chosen stress component at the times of deep moonquakes. Recent works have both expanded the catalog [*Bulow et al.*, 2005, 2007] and reclassified many of its members [*Nakamura*, 2003]. To fully describe deep moonquake failure, all known events from a single cluster should be considered.

1.3.2. Possible Complications in Focal Mechanism Studies

[17] The variations in fault plane orientations resulting from the stress analyses discussed above have precluded definitive interpretation in terms of focal mechanisms. Focal mechanism estimates based on individual event amplitudes [*Nakamura*, 1978] may not be accurate since deep moonquake amplitudes are not well constrained; they can differ among channels on a single station [*Bulow et al.*, 2005]. Similarly, estimates based on S wave arrival polarizations [*Koyama and Nakamura*, 1980] may not be accurate since different plane orientations are obtained when using data from different sets of stations (meaning the result using data from stations 12, 14, and 15 may be different from that obtained using data from stations 14, 15, and 16). In addition, none of the studies that estimated fault parameters provided error bars or uncertainty estimates.

1.3.3. Some General Drawbacks of Previous Works

[18] Often, generalizations about deep moonquakes are made on the basis of the analysis of only a small number of clusters, even though the entire population is known to be distributed over a large geographical area (Figure 1), and different clusters are known to respond to different tidal periods [*Bulow et al.*, 2007]. The most studied cluster is A1, largely because it has the largest number of events and a higher percentage of high-quality (large signal-to-noise ratio) events. A1 is the only cluster common to both the stress studies and the focal mechanism studies mentioned above, being the sole object of the latter.

[19] Another interesting property of A1 events is their observed polarity reversals. During a period of time between 1972 and 1974, some A1 events exhibited polarity opposite to that seen during the rest of the experiment [*Nakamura*, 1978]. Several of the aforementioned stress studies attempted to account for this behavior by introducing a constant ambient stress in addition to the time-varying tidal stress [*Toksöz et al.*, 1977; *Cheng and Toksöz*, 1978]. The A1 cluster may not be representative of all deep moonquake clusters, despite its large number of events,

since only two other cataloged clusters (A20 and A25) out of 319 [*Nakamura et al.*, 1981; *Nakamura*, 2007] have been shown to produce opposite polarity events. While other clusters have been suggested to possess opposite polarity events (Y. Nakamura, personal communication, 2009), these have not been confirmed.

[20] In this paper, we explore the relationship between deep moonquakes and tidal stress and attempt to constrain deep moonquake focal mechanisms by testing a specific hypothesis for failure, which we apply to a large sample of deep moonquake clusters. In section 2, we describe our failure criterion and review the assumptions associated with our Moon model and the formulation of the tidal stress. The implementation of our criterion is discussed in section 3, illustrated using synthetic data to verify functionality. Explicit examples are given for clusters A1 and A37 (although A1 may not be the ideal example cluster for the reasons stated above, we include it for sake of consistency with earlier work). Section 4 summarizes the outcome of our method when applied to a large sample of deep moonquake clusters, tabulates the resulting fault plane orientations, and provides error analysis. A discussion of our findings and a proposed physical mechanism consistent with our observations is presented in section 5.

2. Formulation of the Failure Criterion

[21] We perform a grid search over all possible plane orientations for the fault plane yielding a linear combination of normal (σ_N) and shear (σ_S) stresses that best approximates a constant value at the times of moonquakes from a given cluster. In other words, we solve for the weights w_N and w_S necessary to minimize

$$C - (w_N\sigma_N + w_S\sigma_S) \tag{1}$$

where C is a constant, in a least squares sense (i.e., the set of weights for which the sum of the squared residuals between the model and the observations has its smallest value). This criterion is loosely based on the Coulomb stress criterion

$$\sigma_C = \sigma_S + \mu_f(\sigma_N + P) \tag{2}$$

where μ_f is the friction coefficient and P is the pore pressure, in that we consider relative contributions of shear and normal stress (the pore pressure in the Moon is likely negligible since the water content of the lunar interior is extremely low [*McCubbin et al.*, 2007; *Saal et al.*, 2008]). However, our formulation is more general than the usual Coulomb criterion, in that we do not assume a value for μ_f, a material property that is not well constrained in the lunar interior at the depths of deep moonquakes.

2.1. Model Assumptions

[22] In formulating the tidal stress and our failure criterion, we make the following assumptions:

[23] 1. We consider only the tidal influence of the Earth; tidal stresses raised in the Moon due to the Sun are 7 orders of magnitude smaller (see section 2.2).

[24] 2. In our stress calculations, we assume the Moon has a purely elastic response. Since the viscoelastic relaxation time (on the order of 1000 years given estimates of the lunar mantle viscosity and elastic rigidity) [*Meissner*, 1977; *Stegman et al.*, 2003; *Lammlein*, 1977] is much longer than the forcing period (dominantly 1 month), the elastic approximation is reasonable.

[25] 3. Our stress formulation does not include the hydrostatic pressure at depth owing to the presence of overlaying rock. We assume that deep moonquake failure occurs in response to changes in the tidal stress on preexisting faults, to which the overburden pressure does not contribute.

[26] 4. Because we do not have a unique or well-posed forward model for defining possible ambient stresses (for example, owing to thermal contraction or convection), we assume that deep moonquakes occur solely in response to tidal stress. Incorporating additional parameters into our inversion at this time is not justified by the data.

[27] 5. Our tidal stress calculations assume a homogeneous Moon. As noted by *Minshull and Goulty* [1988], introducing a more realistic layered model with material properties that vary with depth changes only the amplitude and not the phase of the tidal stress at a given location and time. This variation can be absorbed into the weights w_N and w_S in the formulation of our failure criterion, so we opt for a simpler homogeneous model as it drastically reduces the tidal stress computation time.

[28] 6. Because shear stresses in the lunar interior are likely to have been relieved over time by creep processes [*Nakamura*, 1978; *Minshull and Goulty*, 1988], all of our calculations use the demeaned shear stress. In our formulation, this is expressed as the shear stress on a given fault within the Moon due to the Earth at its current position, minus the shear stress on the fault due to the Earth in its mean position.

[29] 7. We assume that deep moonquakes can be explained by a threshold criterion. As we shall see, in some cases, other types of failure may describe deep moonquakes more appropriately.

[30] 8. Deep moonquakes have been estimated to have stress drops of approximately 0.1 bars [*Goins et al.*, 1981] or 10 kPa. However, our failure criterion assumes that moonquakes do not change the stress function by relieving stress. The estimated stress drops are on the same order of magnitude as the peak-to-peak monthly tidal stress variation. If we include stress drops in our criterion such that a certain percentage of stress is relieved when the threshold is reached, a few events would quickly relieve the stress to a point where the threshold would never be reached again, and moonquakes would cease. This effect results from the constant mean nature of the sinusoidally varying tidal stress: there is no perpetually increasing (e.g., tectonic) stress term. The timing of moonquake cessation would depend on the assumed stress drop, taking anywhere from days to months. However, deep moonquake occurrence was observed throughout the 8-year duration of the Apollo experiment.

2.2. Tidal Stress Calculation

[31] Following the method initiated by *Love* [1967] and refined by *Alterman et al.* [1959], we compute tidal stresses within the Moon due to elastic deformation. For more recent presentations, see, for example, *Wu and Peltier* [1982] and *Sabadini and Vermeersen* [2004].

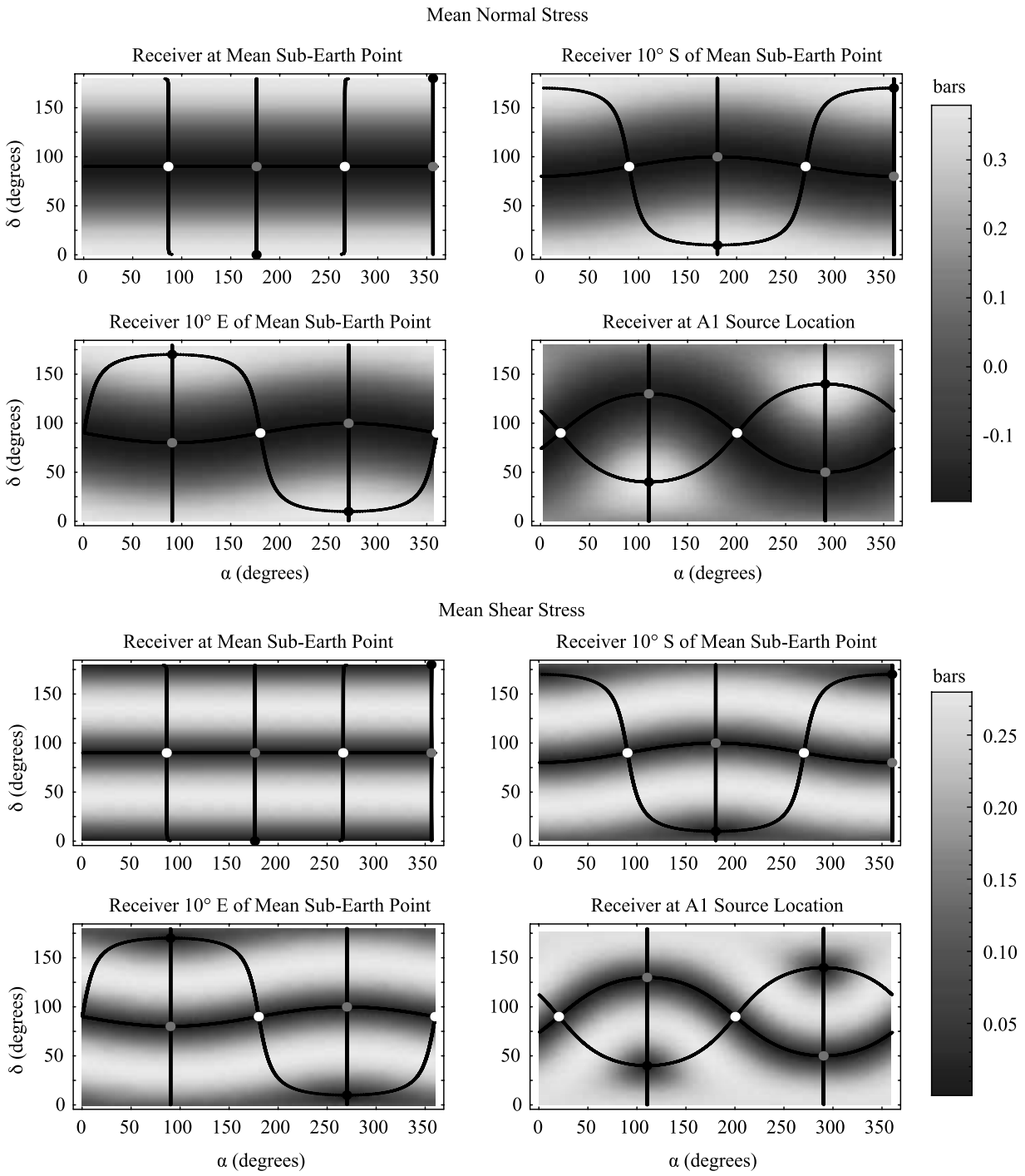

Figure 2. (top) Normal and (bottom) shear tidal stresses raised by the Earth in its mean position, resolved on all possible plane orientations at four receiver positions. The positions are (1) receiver at mean sub-Earth point, (2) receiver 10°E of mean sub-Earth point, (3) receiver 10°S of mean sub-Earth point, and (4) receiver at A1 source location. The maximum, intermediate, and minimum principal stress directions are shown for comparison (black, white, and grey dots, respectively). The dark lines mark the planes joining the principal stress directions.

[32] The gravitational interaction between the Moon and the Earth causes deformation on both bodies. The amplitude of the tidal deformation on and in the Moon is determined by the gravitational potential Φ of the tide-raising body (the Earth) and the internal structure of the Moon. The Earth-induced gravitational potential at any point within the Moon (r, θ, ϕ) satisfies Laplace's equation and can be expressed as a spherical harmonic expansion:

$$\Phi = -\frac{GM_E}{r_s} \sum_{n=0}^{\infty} \left(\frac{r}{r_s}\right)^n P_n(\cos \Delta) \tag{3}$$

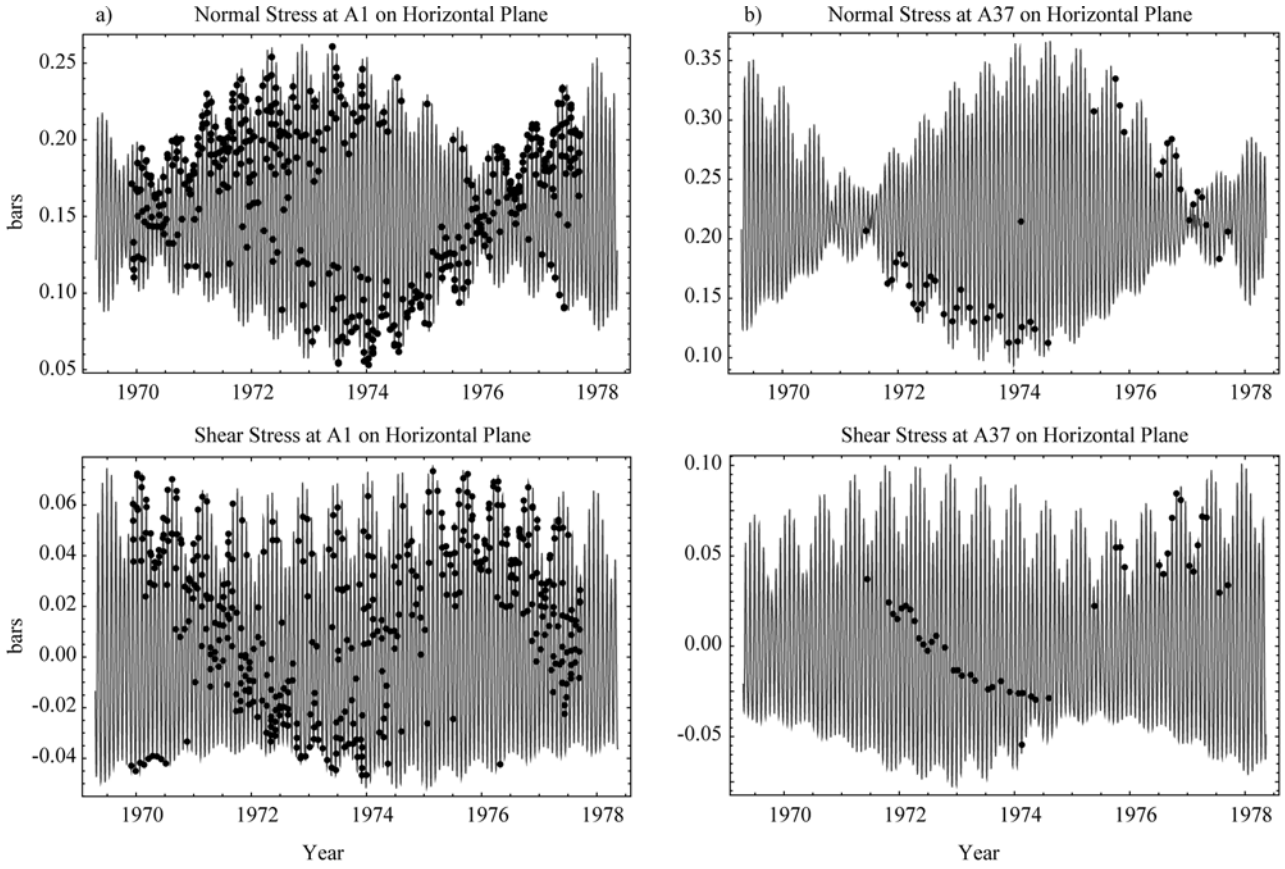

Figure 3. (a) Normal (top) and shear (bottom) tidal stresses evaluated at the A1 location (latitude −15.7°N, longitude −36.6°E) on a horizontal plane (δ, α = 0°, 0°) as the Earth moves relative to the Moon during the course of the Apollo experiment. In this and Figures 5 and 9, the sinusoidally varying black line shows stresses evaluated on uniform 1-day time steps, and the dots show stresses at the times of (A1) moonquakes. (b) Stresses evaluated on a horizontal plane at the A37 location (latitude 22.5°N, longitude 29.7°E).

where G is the gravitational constant, M_E is the mass of the Earth, r_s is the (time-varying) distance from the center of the Moon (the origin) to the center of the Earth, r is the radial distance within the Moon measured from the origin, and $P_n(x)$ is a Legendre polynomial of degree n. The angle Δ is the angle between the point (r, θ, ϕ) within the Moon and the position of the Earth (r_s, θ_s, ϕ_s) such that $\cos\Delta = \cos\theta\cos\theta_s + \sin\theta\sin\theta_s\cos(\phi - \phi_s)$, where θ and θ_s are selenographic (Moon-centered) colatitudes (zero at the north pole of the Moon), and ϕ and ϕ_s are selenographic longitudes (increasing to the East from the lunar meridian).

[33] We are interested in tidal deformation, which is dominated by the terms of harmonic degree $n = 2$. The imposed potential can be written

$$\Phi_2 = \frac{GM_E r^2}{2r_s^3}\left(1 - 3\cos^2\Delta\right) \tag{4}$$

The magnitude of the degree two tidal potential of the Earth compared to that of the Sun can be estimated using the following ratios. The Sun/Earth mass ratio $M_{ratio} = M_S/M_E \approx 3 \times 10^{-6}$. The mean Sun/Earth distance ratio $r_{ratio} = a_S/a_E \approx 2.6 \times 10^{-3}$. Following equation (4), the comparative Earth/Sun magnitude of the degree two tidal potential is $M_{ratio}/r_{ratio}^3 \approx 171$. However, the stress depends on the second derivative of the potential (see Appendix A), yielding $M_{ratio}/r_{ratio}^5 \approx 2.5\times10^7$, which indicates that the tidal influence of the Earth is 7 orders of magnitude larger than that of the Sun. We therefore neglect the tidal influence of the Sun. Deformation caused by the imposed potential of the Earth will affect displacements, strains, stresses, and changes in the Moon's gravitational potential. The elastic constitutive relation states that stresses are linearly related to strains:

$$\sigma_{ij} = \lambda\epsilon_{kk}\delta_{ij} + 2\mu\epsilon_{ij} \tag{5}$$

where σ_{ij} is the stress tensor, ϵ_{ij} is the strain tensor, λ and μ are the Lamé parameters, and δ_{ij} is the unit diagonal tensor. We compute the stress σ_{ij} due to tidal deformation $\mathbf{u} = (u_r, u_\theta, u_\phi)$ in a tensor form that can be evaluated at any time, at any place within the Moon, owing to the time-varying position of the Earth (see Appendix A).

[34] The stress tensor is a symmetric 3 × 3 matrix, and in the coordinate system (1, 2, 3) can be written as

$$\sigma_{ij} = \begin{bmatrix} \sigma_{11} & \sigma_{12} & \sigma_{13} \\ \sigma_{12} & \sigma_{22} & \sigma_{23} \\ \sigma_{13} & \sigma_{23} & \sigma_{33} \end{bmatrix} \tag{6}$$

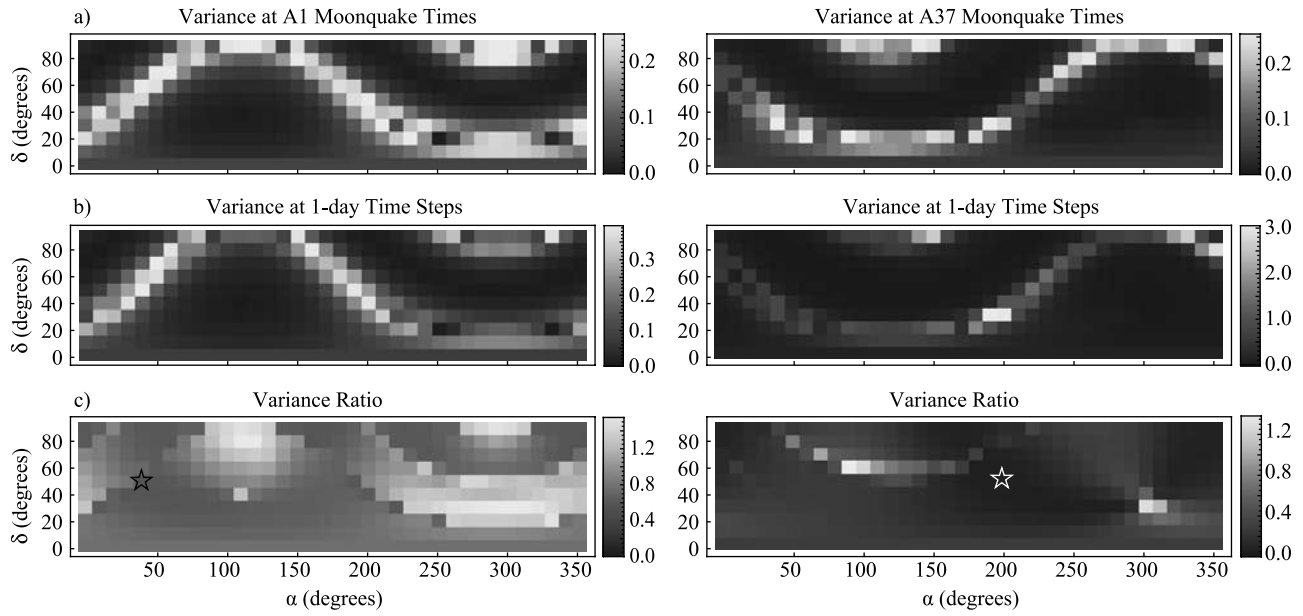

Figure 4. Variance of the linear combination of normal and shear stresses at each (δ, α) element that minimizes equation (1), with C equal to 1 bar (100 kPa). (a) Variance at A1 (left) and A37 (right) moonquake times. (b) Variance at uniform 1-day time steps. (c) Variance ratio. The grid element where the variance ratio is minimum (0.58 for A1, 0.06 for A37) is marked with a star and corresponds to the best fit failure plane.

It has the defining property that for a plane specified by unit normal vector $\hat{\mathbf{u}}$, the force per unit area acting across that plane (the traction) is given by

$$\mathbf{t} = \sigma_{ij} \cdot \hat{\mathbf{u}} \tag{7}$$

The traction can be written as the sum of two components, one of them (the normal stress vector $\mathbf{n}$) perpendicular to the plane, and the other (the shear stress vector $\mathbf{s}$) in the plane. The normal component of the traction vector (the normal stress) is

$$n = \hat{\mathbf{u}} \cdot \mathbf{t} = \hat{\mathbf{u}} \cdot \sigma_{ij} \cdot \hat{\mathbf{u}} \tag{8}$$

and the normal stress vector is $\mathbf{n} = n\hat{\mathbf{u}}$. The shear stress vector is $\mathbf{s} = \mathbf{t} - \mathbf{n}$ and the magnitude of this vector (the shear stress) is

$$s = \sqrt{\mathbf{s} \cdot \mathbf{s}} \tag{9}$$

To compute shear and normal stress at the deep moonquake hypocenters, we must specify a failure plane orientation. The plane is defined by a local unit normal vector $\hat{\mathbf{u}}$ with a dip δ and strike α. Note that a vertical unit normal vector ($\delta = 0°$) corresponds to a locally horizontal failure plane. The dip of the plane increases to the south from horizontal and the strike increases counterclockwise from south, when viewed from above. The entire suite of possible plane orientations can be described with δ ranging from 0 to 90° and α from 0 to 360°. It is not necessary to extend δ to 180°, since a plane defined by a given unit normal is the same plane as defined by the negative of that unit normal.

[35] In Figure 2, we show the normal and shear stress computed over all possible plane orientations at four different receiver locations, as raised by the Earth in its mean position at a single point in time. At the four locations, each shear stress plot represents the mean stress field that is removed from the instantaneous stress field in the demeaning process. Also shown are the principal stress directions (eigenvectors corresponding to the maximum, intermediate, and minimum eigenvalues of the stress tensor). As defined, the principal stress directions represent the normal vectors to those planes in which the shear stress is zero.

[36] We are interested in determining whether temporal variations in shear and normal tidal stress can be linked to moonquake occurrence times. For example, the normal and shear stresses resolved on a locally horizontal plane at the A1 source location (as suggested by *Nakamura* [1978]) with the Earth moving relative to the Moon over the course of the Apollo experiment are shown in Figure 3a. For comparison, those computed on a horizontal plane at the A37 source are shown in Figure 3b. For both clusters, the individual stresses resolved on a horizontal plane are not consistent with threshold-type failure at moonquake times, since the moonquakes do not consistently occur at a constant stress level.

3. Implementation of the Failure Criterion

[37] In equation (1), any constant stress C can be chosen, since the resulting linear combination can be changed with a scale factor. We use C = 1 bar (100 kPa). On a grid of all possible plane orientations, with 10° intervals of dip δ and strike α, we search for the linear combination of normal and shear stress such that the ratio of variances computed at quake times and at uniform time steps is minimized. In other words, at each (δ, α) grid element, we solve for the coefficients w_N and w_S necessary to minimize equation (1). Using those coefficients, we then compute the linear combination of σ_N and σ_S at each grid element. We define the

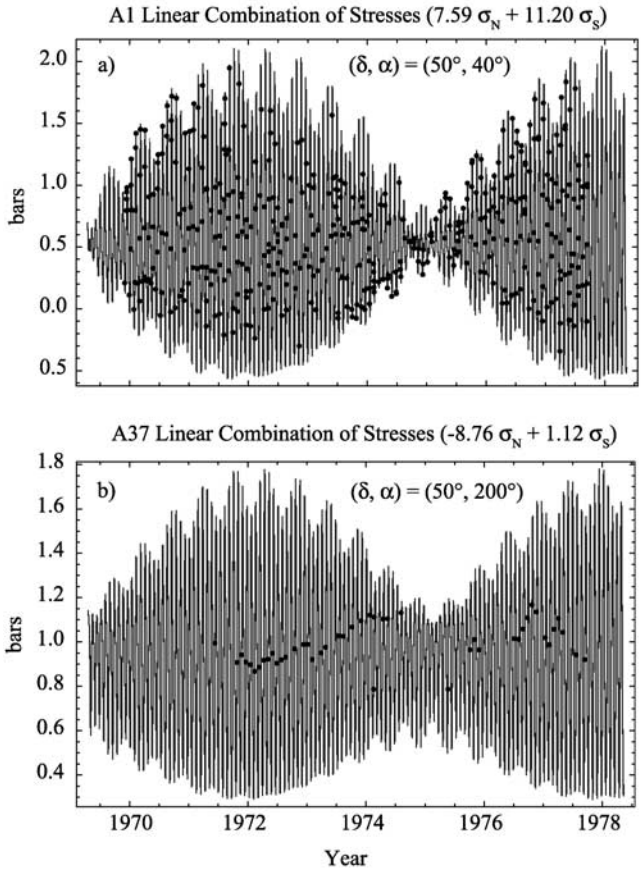

Figure 5. (a) Linear combination of normal and shear stresses such that $7.59\ \sigma_N + 11.2\ \sigma_S \simeq 1$ computed on the plane with $\delta = 50°$ and $\alpha = 40°$ at the A1 source. The dots represent the value of the linear combination at A1 moonquake times and do not seem to approximate a more constant value than the individual stresses computed on a horizontal plane. (b) Linear combination of normal and shear stresses such that $-8.76\ \sigma_N + 1.12\ \sigma_S \simeq 1$ computed on the plane with $\delta = 50°$ and $\alpha = 200°$ at the A37 source. The dots represent the value of the linear combination at A37 moonquake times and group close to 1 bar (100 kPa) as computed.

best fit plane orientation as the one that minimizes the ratio of the variance of the best fitting linear combination at quake times to the variance of said linear combination at 1-day time steps. Using the variance ratio as the test statistic removes the bias associated with the uneven temporal distribution of moonquakes.

[38] To ensure that the grid search behaves as expected, we first test our formulation using a synthetic time series. Using known values for the fault dip and strike (δ_1, α_1) at a given location and depth within the Moon, we compute the shear stress resolved on that plane, and create a series of synthetic event times such that the shear stress is equal to a given constant C_1. We then input these event times into our grid search formulation. As expected, we recover the same plane orientation as we put in, with weights w_N and w_S equal to zero and C/C_1, respectively, such that equation (1) is satisfied at each synthetic event time.

[39] We now apply our technique to the deep moonquake data, beginning with our example clusters A1 and A37. The variance of the linear combination of σ_N and σ_S at moonquake times, as a function of δ and α, is shown in Figure 4a for A1 (left) and A37 (right). The variance at 1-day time steps is shown in Figure 4b, and the ratio of a to b is shown in Figure 4c. Each (δ, α) grid element is associated with a different pair of weights w_N and w_S, not shown. Because we evaluate a different linear combination of stresses at every plane orientation, and since each linear combination is evaluated at many times, the plots in Figure 4 do not vary smoothly as do the plots of normal and shear stress owing to a stress tensor at a single point in time (Figure 2).

[40] In Figure 4c, the minimum variance ratio, indicating the best fitting linear combination of shear and normal stress, is marked with a star. For A1, the minimum variance ratio is 0.58, the weights w_N and w_S are 7.59 and 11.20 respectively, and (δ, α) = (50°, 40°). For A37, the minimum variance ratio is 0.06, the weights w_N and w_S are −8.76 and 1.12 respectively, and (δ, α) = (50°, 200°). The resulting linear combinations are shown in Figure 5. Note that the best fitting linear combination of stresses at the times of A1 moonquakes does not provide an obviously improved fit to our criterion (equation (1)) compared with the individual components of stress computed on a horizontal plane (Figure 3a). A37 moonquakes seem better suited to a threshold-type criterion.

[41] It should be noted that 10° intervals of dip and strike do not uniformly sample (δ, α) space. In Figure 6, we show the three-dimensional hemisphere that is formed by the unit normal vectors representing each (δ, α) pair in the two-

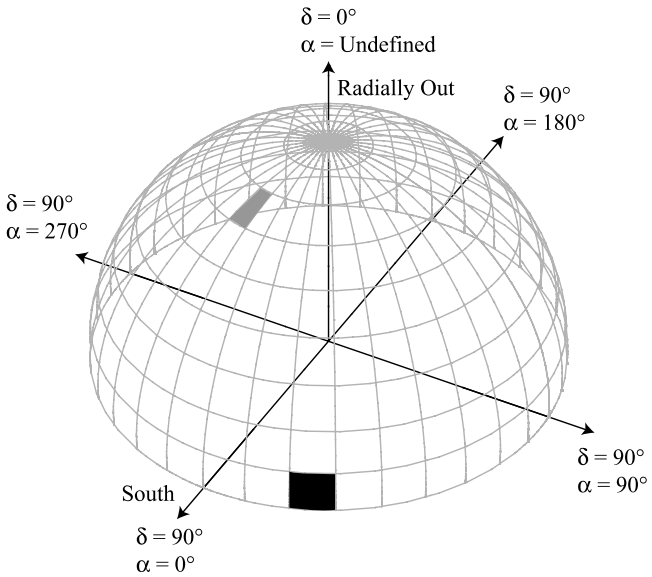

Figure 6. Three-dimensional hemisphere formed by the unit normal vectors representing each (δ, α) pair in the two-dimensional plots shown in Figure 4, with 10° intervals of dip and strike. The dip of the plane increases to the south from horizontal and the strike increases counterclockwise from south, when viewed from above. Note that the surface area spanned by each grid element is not uniform and depends on the dip (compare, e.g., the black element and the grey element).

Table 1. Grid Search Results: Normal and Shear Stress[a]

Cluster	Number of Events	Latitude (deg)	Longitude (deg)	Depth (km)	Minimum Variance Ratio	M Ratio	δ (deg)	α (deg)	w_N	w_S
A1	441	−15.7	−36.6	867	0.57	2.7	50	40	7.59	11.20
A3	42	−2.9	−50.3	946	0.28	6.7	70	260	−20.21	8.09
A6	178	43.5	55.5	844	0.52	2.2	20	140	−4.42	−1.09
A7	85	25	53.2	893	0.17	6.9	10	190	−18.00	9.65
A8	327	−23.7	−35.5	1086	0.39	2.4	80	20	−2.01	−2.17
A9	145	−6	−19.7	1037	0.19	3.1	20	110	1.59	−2.83
A10	230	−35.7	−40.3	988	0.36	2.7	40	300	−2.05	−2.43
A13	57	−19.1	−41.7	973	0.18	3.5	60	240	−3.07	−1.63
A14	165	−29.6	−44.4	933	0.24	5.3	60	90	3.45	0.38
A15	50	0.7	−3.9	747	0.36	1.2	80	220	−5.55	1.01
A16	50	7.5	6.3	1019	0.15	2.7	80	110	−4.90	−2.83
A17	49	25.5	−21.9	807	0.02	25.8	60	240	−4.78	−1.44
A18	214	23.3	32.7	925	0.18	4.6	70	50	−2.80	−1.92
A19	45	27.7	34.4	974	0.02	24.3	60	330	3.21	1.50
A20	153	23.7	−31.4	945	0.41	3.1	40	130	8.64	1.37
A21	69	−18.2	−50.8	1037	0.13	8.4	50	240	−1.38	−2.64
A22	48	21.6	43.6	788	0.01	114.9	80	20	−1.85	−2.57
A25	72	35.1	59.8	924	0.09	3.5	40	50	−3.81	−1.84
A26	54	14.3	5.2	1122	0.52	1.9	10	320	2.12	−1.17
A30	45	12.7	−35.7	931	0.16	6.3	80	170	−2.23	−2.01
A32	35	25	43.6	944	0.16	6.7	70	40	−3.65	−1.44
A33	57	5.1	115.8	877	0.07	9.3	10	240	−7.73	−0.63
A34	39	6.8	−7.2	971	0.07	5.8	20	290	4.60	−0.55
A36	43	27.5	−4.6	1058	0.22	3.3	20	30	2.19	−1.10
A37	46	22.5	29.7	1343	0.06	24.2	50	200	−8.76	1.12
A38	41	7.8	43.3	1031	0.51	2.2	50	130	−2.48	−1.79
A40	35	−1.3	−10.3	867	0.13	2.6	20	120	2.64	−0.61
A41	44	13.8	−29.2	847	0.06	10.4	40	100	3.07	0.05
A42	50	22.2	−50.7	907	0.13	9.6	30	130	11.33	0.74
A44	86	50.2	60.2	908	0.38	2.3	20	70	−3.32	−2.66
A51	50	12.3	37.7	1125	0.12	4.5	70	40	−1.20	−2.58
A65	35	46.6	42.3	861	0.09	6.5	10	170	−10.89	2.93
A73	36	21.1	−44	908	0.15	14.2	30	80	2.80	−1.49
A96	36	6.2	11.9	794	0.06	25.4	30	240	4.08	−1.83
A97	44	−8.4	17.9	989	0.08	19.8	50	20	−10.05	1.67
A202	36	1	2.8	919	0.22	3.0	10	290	2.00	2.32
A234	44	36.8	21.2	1006	0.12	6.0	80	220	−1.99	−2.21
A238	36	26.3	20	831	0.05	21.7	50	350	4.05	−0.58
A257	45	35	19.1	1063	0.13	6.2	50	50	−16.40	−1.34

[a]Boldface type indicates clusters meeting our final criteria for goodness of fit; see section 4.2.

dimensional plots shown in Figure 4. A horizontal plane is one with a dip of 0°, where the strike is undefined. In the selenographic coordinate system, the corresponding normal vector points radially outward at each cluster location. Note that in three dimensions, the surface areas of each 10° by 10° grid element are not equal; they depend on the dip. Fault plane orientations with smaller dip values (e.g., closer to horizontal) are more finely sampled in area than those with large dip values (e.g., near-vertical failure planes).

4. Results: Summary and Interpretation

[42] We now apply our grid search to 39 deep moonquake clusters (Figure 1), including the two presented previously. The 39 clusters are those having more than 35 cataloged events [*Nakamura et al.*, 1981] and location errors (with respect to a specific velocity model) less than or equal to 10° in latitude and longitude [*Nakamura*, 2005]. We chose the well-located clusters since the tidal stress calculation is location-specific. Although cluster A14 does not meet the location error criterion, we include it because it is one of the clusters for which new events have recently been discovered [*Bulow et al.*, 2007].

[43] For each cluster, we report the value of the minimum variance ratio, the weights w_N and w_S for the best fitting linear combination of normal and shear stress, and the corresponding plane orientation (δ, α) in Table 1. Some overall characteristics of these results are summarized below.

[44] 1. For some clusters, our grid search identifies planes conducive to failure, on the basis of the value of the minimum variance ratio. A significant number of clusters have minimum variance ratios that are small, indicating we were able to find a stress state that is approximately constant at moonquake times. As shown in Figure 7a, 12 out of 39 (31%) clusters have minimum variance ratios less than 0.1. Of these 12 clusters, eight (67%) have maximum variance ratios at least 1 order of magnitude larger than the corresponding minimum variance ratio, suggesting that the best fitting failure plane is distinct from other planes. We refer to this measure as the "M ratio," also listed for each cluster in Table 1:

$$\text{M ratio} = \frac{\textit{maximum variance ratio}}{\textit{minimum variance ratio}} \tag{10}$$

This result suggests that some deep moonquake clusters are well explained by Coulomb-like failure on a plane.

[45] 2. We note that the ratio of w_S to w_N (an "effective" friction factor, μ_f) is not constant among clusters (Figure 7b), indicating either that the lunar interior is heterogeneous (widely accepted, but not accounted for in our modeling) or that our failure criterion is inadequate to describe deep moon-

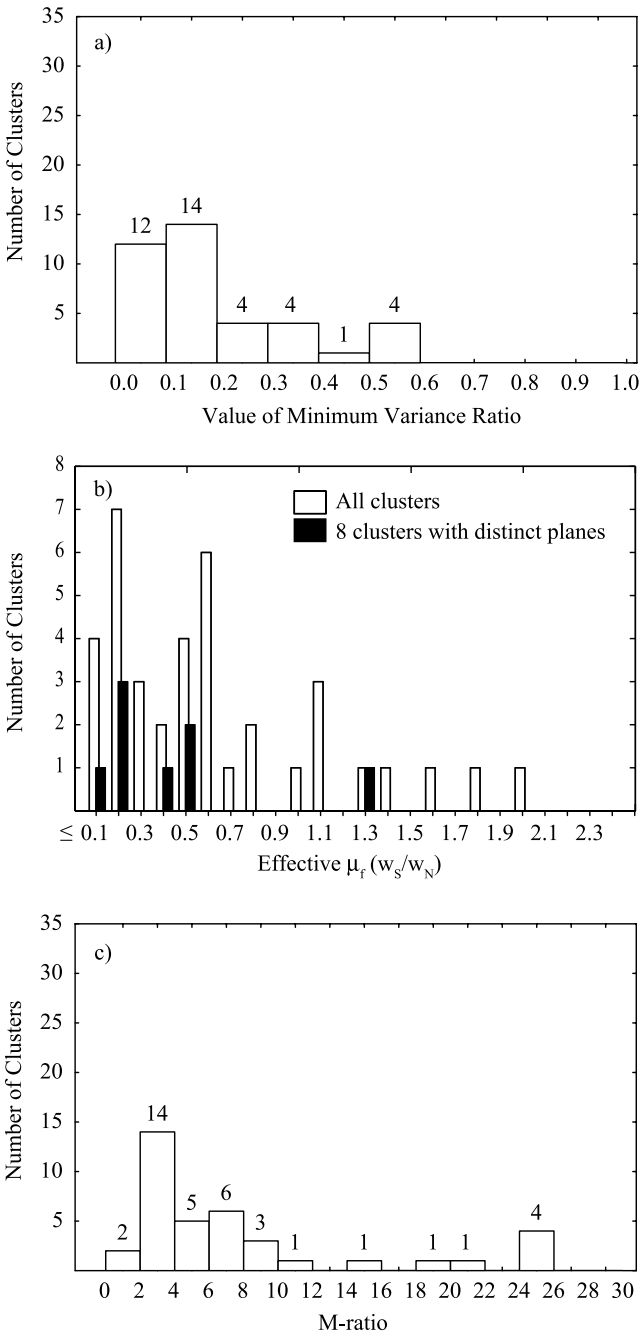

Figure 7. (a) The value of the minimum variance ratio achieved for each of the 39 clusters analyzed. (b) The value of the effective friction factor for each of the 39 clusters (white) and for those 8 clusters with well-constrained failure planes (black). We note that the range of values spanned by the well-constrained clusters is similar to that of all clusters. (c) The value of the M ratio computed for each of the 39 clusters. Note that one cluster is missing from the plot because its ratio of maximum to minimum variance ratio has a value much greater than the others (∼114).

quakes (which contradicts point #1 above). We conclude that factors in addition to (or other than) tidally driven shear failure on a plane may better describe some deep moonquakes.

[46] 3. For some clusters, failure does not depend heavily on plane orientation, indicated by small M ratios (see Figure 7c). For these clusters the variance ratios for all values of strike and dip are similar (i.e., a single plane orientation significantly "better" than the rest could not be found). This result also suggests that failure on a plane due to tidal stresses may be inadequate to explain deep moonquakes.

[47] 4. Some clusters respond more strongly to the normal stress level than to the shear stress level, as evidenced by the values for w_N and w_S: 19 out of 39 clusters (49%) have $|w_N| > |w_S|$. Interestingly, among the eight previously mentioned clusters with distinct failure planes, seven have $|w_N| > |w_S|$. This result suggests that a pressure-related phenomenon may be contributing to deep moonquake failure.

[48] 5. Fault plane orientations are different for nearby clusters on the basis of the directions of the fault plane normal vectors. A 3D plot of the best fitting fault plane normal vectors is shown in Figure 8. For comparison, normal vectors representing nearly uniform plane orientations (with ±10° noise in the strike/dip) are also shown at the location of each cluster. Failure appears to be locally determined, rather than reflecting large-scale structures in the lunar interior.

[49] These results partially support our failure hypothesis, but also suggest that factors other than elastic tidal stress may be contributing to failure. Previous studies suggested that ambient stresses might be involved, such as elastic stresses preserved in the interior due to early lunar events (e.g., bombardment or possible early tectonics), convective stresses in the deep interior [*Toksöz et al.*, 1977], or thermal stresses resulting from contraction as the lunar interior cools [*Minshull and Goulty*, 1988]. Since investigation of such models requires a large parameter search, and our main constraints on deep moonquakes are simply their times of occurrence, we do not pursue the role of ambient stresses here.

[50] Another factor that may play a role in deep moonquake occurrence is the rate of stress, which we now investigate. This investigation is motivated by the work of *Bills et al.* [2008] and *Bulow* [2007], who found that moonquake times at some clusters correspond strongly to the rate of change of the parameters describing the position of the Earth relative to the Moon. This suggests that the Moon may be responding viscoelastically to the imposed tidal stresses (i.e., there may be a delay between the optimum failure conditions and the actual onset of failure). As an alternative to the more complicated viscoelastic stress calculations, we investigate the relevance of stress rates by adapting our failure criterion.

4.1. Possible Importance of Stress Rates

[51] We estimate the relative importance of stress rates by modifying our failure criterion to include their influence:

$$C - \left(w_N\sigma_N + w_S\sigma_S + w_{\dot{N}}\dot{\sigma}_N + w_{\dot{S}}\dot{\sigma}_S\right) \qquad (11)$$

where the dot indicates a time derivative. To compute the stress rates, we first compute the shear and normal stress on a given plane at uniform time steps. These time series are then interpolated with cubic splines of the dependent variable (time), so their derivatives can be computed analytically. The resulting functions can then be evaluated at both uniform time steps and at moonquake times. Shear and normal stress rates on locally horizontal planes at the A1 and A37 source locations over the course of the Apollo experiment are shown in Figure 9, along with the minimum

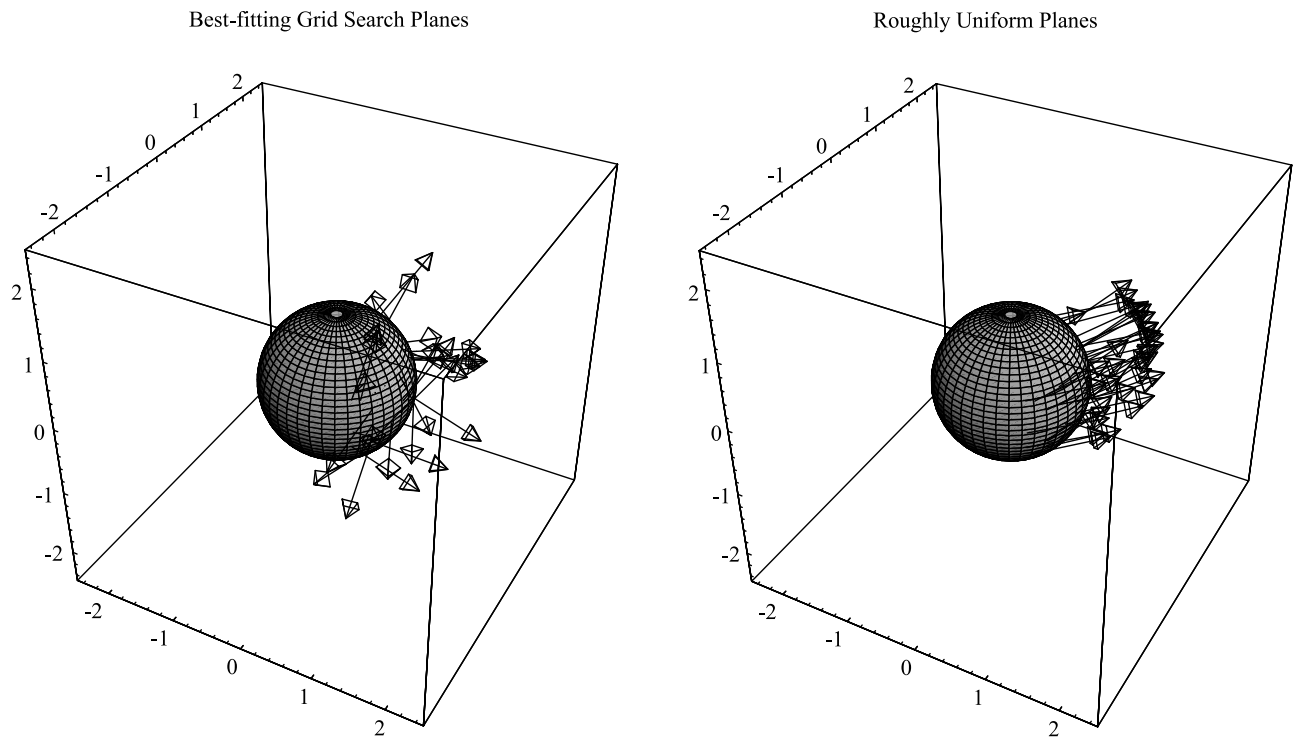

Figure 8. (left) At each cluster location on a unit sphere (constant depth assumed for plotting purposes) the best fitting fault plane normal vectors are shown. (right) For comparison, normal vectors representing nearly uniform plane orientations (with ±10° noise in the strike/dip) are also shown at the location of each cluster.

variance ratio maps associated with the grid search including the rates, and the resulting best fitting linear combination that satisfies equation (11) (again with C = 1 bar or 100 kPa). Note that the stress rate weights $w_{\dot{N}}$ and $w_{\dot{S}}$ must have units of time for equation (11) to hold with C having units of stress.

[52] For each of our 39 clusters, we report the value of the minimum variance ratio, the weights w_N, w_S, $w_{\dot{N}}$ and $w_{\dot{S}}$ for the best fitting linear combination of shear and normal stresses and rates, and the corresponding plane orientation (δ, α) in Table 2. Using this revised failure criterion, we observe that a larger percentage (27 out of 39, or 69%) of clusters now possess minimum variance ratios less than 0.1. In addition, 25 out of those 27 clusters (93%) have M ratios greater than 10. These results suggest that deep moonquakes respond significantly to stress rates. However, it is important to note that including the stress rates in the failure criterion will always produce improved (lower) minimum variance ratios, because in that case there are four variables in the fit, rather than two.

[53] To judge the relative importance of stress rates, we must determine which criterion (equations (1) or (11)) results in a better-constrained minimum variance ratio. For a given cluster, we compare the hemispherical area covered by those (δ, α) grid elements with variance ratios less than or equal to 1.05 times the minimum value, for each of the two criteria. To calculate the surface area, we map the two-dimensional (δ, α) variance ratio plots (e.g., Figure 4) onto a hemisphere (Figure 6), and then calculate the summed area contributed by all grid elements whose variance ratio is less than or equal to 1.05 times the minimum variance ratio. The best fit criterion is defined as the one for which the combined surface area of those grid elements is minimized.

[54] Results for both failure criteria are listed in Table 3 for each cluster (values are given as a percentage of the total hemispherical surface area). In Table 3, the ten clusters with stars are those for which the surface areas spanned by the grid elements with variance ratios less than or equal to 1.05 times the minimum value for both failure criteria were equal, meaning that equations (1) and (11) performed equally well as the failure criterion. On the basis of the values in Table 3, the minimum variance ratios for 21 out of the remaining 29 clusters are better constrained using equation (11) (stresses and rates) as the failure criterion, while eight are better constrained using equation (1) (just stresses). If we expand the cutoff to 1.10 times the minimum variance ratio, a larger number of clusters respond favorably to equation (11) (stresses and rates).

4.2. Fault Plane Orientation Uncertainties

[55] To estimate the uncertainties in our best fit fault plane orientations, we determine the total spatial extent of all grid elements with values less than or equal to 1.05 times the minimum value. We consider only the 29 clusters for which a distinction can be made between using equations (1) and (11) as the failure criterion. In Table 3, clusters in bold are those for which all grid elements corresponding to less than or equal to 1.05 times the minimum variance ratio reside in a single local minimum. These 22 clusters are thus assigned fault plane orientation uncertainties in multiples of ±10° in both dip and strike, corresponding to the resolution of our grid search. Of these, six (A9, A17, A22, A26, A73, and A202) were best fit by equation (1), and 16 were best fit by equation (11).

[56] The remaining seven clusters are those for which there are multiple local minima corresponding to 1.05 times

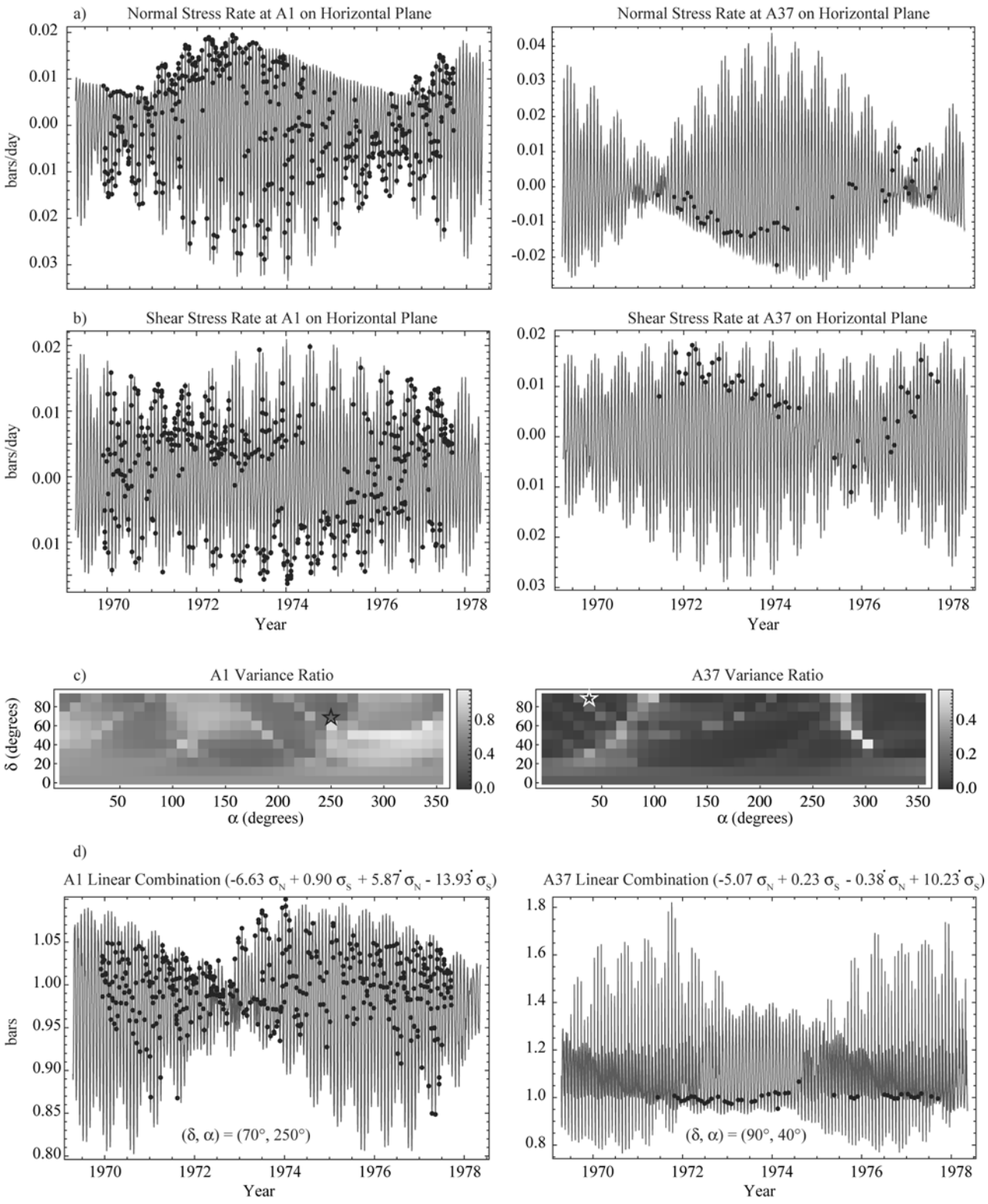

Figure 9. (a) Normal and (b) shear stress rates (in bars/day) evaluated at the A1 (left) and A37 (right) locations on locally horizontal planes (δ, α = 0°, 0°). (c) Variance ratio of the linear combination of normal and shear stresses and stress rates at each (δ, α) element that minimizes equation (11), with C equal to 1 bar (100 kPa), for A1 (left) and A37 (right). The minimum in each case is marked with a star. (d) Linear combination of normal and shear stresses and rates such that $w_N \sigma_N + w_S \sigma_S + w_{\dot{N}} \dot{\sigma}_N + w_{\dot{S}} \dot{\sigma}_S \simeq 1$, where $w_N = -6.63$, $w_S = 0.40$, $w_{\dot{N}} = 5.87$ days, and $w_{\dot{S}} = -13.93$ days, computed on the plane with $\delta = 70°$ and $\alpha = 250°$ at the A1 source (left). For A37, the values are $w_N = -5.07$, $w_S = 0.23$, $w_{\dot{N}} = -0.38$ days, and $w_{\dot{S}} = 10.23$ days, with $\delta = 90°$ and $\alpha = 40°$.

Table 2. Grid Search Results: Normal and Shear Stresses and Rates[a]

Cluster	Minimum Variance Ratio	M Ratio	δ (deg)	α (deg)	w_N	w_S	$w_{\dot{N}}$ (days)	$w_{\dot{S}}$ (days)
A1	0.35	3.3	70	250	−6.63	0.40	5.87	−13.93
A3	0.17	7.5	60	260	−7.74	−0.23	16.13	−21.83
A6	0.28	3.4	50	50	−1.79	−3.90	−21.29	8.22
A7	0.04	14.2	60	40	−4.85	−0.18	−3.67	8.97
A8	0.32	2.7	80	240	−5.83	0.43	4.99	−13.29
A9	0.05	13.7	80	120	−9.78	12.95	−38.10	−21.74
A10	0.21	4.5	50	50	−4.62	−1.69	−79.56	31.94
A13	0.10	7.8	50	240	−5.52	0.12	−4.57	10.88
A14	0.15	8.7	80	250	−17.90	11.65	−24.78	−41.06
A15	0.06	10.9	80	270	−6.56	−0.19	−5.30	12.01
A16	0.00	104.4	80	90	−5.42	0.61	−6.15	−10.23
A17	0.00	73.8	90	30	−4.46	−10.98	77.59	−1.29
A18	0.10	6.9	60	80	−3.12	−1.62	−12.65	8.36
A19	0.00	92.6	70	60	−4.20	−0.38	−3.49	4.93
A20	0.30	3.6	40	70	2.22	−0.76	1.19	5.34
A21	0.01	63.8	40	240	−6.48	1.12	5.38	13.19
A22	0.00	80.2	80	340	−14.05	−8.26	49.06	−6.59
A25	0.07	10.8	30	90	−4.66	−1.23	−11.98	−3.32
A26	0.34	3.4	80	40	−6.25	1.57	1.48	−10.65
A30	0.04	17.3	40	60	2.31	−0.57	−2.12	−7.48
A32	0.04	12.5	40	150	−6.83	0.52	16.94	−18.21
A33	0.04	12.8	20	290	−6.82	1.17	3.01	13.44
A34	0.02	14.3	40	80	1.50	4.03	−9.30	14.02
A36	0.03	28.1	90	60	−8.44	2.78	−2.49	−17.56
A37	0.01	46.7	90	40	−5.07	0.23	−0.38	10.23
A38	0.33	3.9	20	30	19.06	−40.03	115.19	25.41
A40	0.04	29.6	20	100	2.79	−0.75	1.14	8.99
A41	0.01	68.8	40	80	2.27	−1.50	2.63	4.71
A42	0.08	10.1	40	220	−1.55	−3.07	14.13	−0.74
A44	0.16	5.5	70	300	2.52	−0.54	−1.24	8.93
A51	0.03	18.8	60	80	−6.77	1.48	6.63	13.72
A65	0.03	20.8	50	320	2.72	−0.96	−0.27	10.69
A73	0.14	10.1	40	80	2.15	−1.58	2.61	0.42
A96	0.04	25.9	20	270	2.54	−0.51	−10.19	−21.98
A97	0.04	19.9	70	50	−0.62	−5.75	9.08	−2.56
A202	0.08	5.8	80	90	−5.18	1.92	−6.96	−8.72
A234	0.01	67.2	80	70	−5.23	0.23	1.27	11.47
A238	0.00	113.6	90	20	−15.42	5.11	−14.64	−53.98
A257	0.02	29.8	80	80	−5.44	0.42	1.24	11.39

[a]Boldface type indicates clusters meeting our final criteria for goodness of fit; see section 4.2.

the value of the minimum variance ratio. This could be an indication that some deep moonquake activity is more complex than can be explained using our threshold plane failure model. Thus we do not estimate fault plane uncertainties for those clusters.

[57] If we combine our various requirements for goodness of fit (value of minimum variance ratio less than 0.1, value of M ratio greater than 10, and ability to assign fault plane uncertainties), we observe that two clusters are well fit by a linear combination of normal and shear stress (equation (1)) and eleven clusters are well fit by a linear combination of normal and shear stresses and stress rates (equation (11)). These clusters are noted in bold face in Tables 1 and 2, and marked with open circles on Figure 1. We note that these clusters are not confined to a particular region. The average number of moonquakes among these 13 clusters is 48, compared to an average of 87 events per cluster for all 39 clusters tested.

5. Discussion

[58] While it is encouraging that our threshold failure criterion can describe failure at some clusters, it is important to note that the method fails for some of the clusters with large event numbers (e.g., A1, A8), which tend to be the best-located clusters. We should expect the best results at such clusters, since the tidal stress calculation is location-dependent. Clearly one or more of our model assumptions is inappropriate. However, as we have already discussed, some of our results seem to indicate that a physical process other than or in addition to the simple buildup and release of tidal stress may be responsible for deep moonquake generation at the remaining clusters.

[59] It is possible that deep moonquakes may be similar to deep earthquakes, which occur in a regime within the Earth where brittle shear failure on a plane is not expected. Laboratory experiments have shown that above a critical pressure and temperature, rocks fail by ductile flow rather than brittle rupture [*Evans et al.*, 1990, and references therein]. In the Earth, this brittle-ductile transition occurs between 10 and 50 km depth (pressure 0.2–1.4 GPa) [*Bott*, 1982], where the corresponding temperature range is approximately 400 to 1000°C [*Stacey*, 1992]. However, a significant number of earthquakes have been observed at much greater depths, between 60 and 700 km beneath the surface [*Frohlich*, 1989], where the pressures and temperatures range from 1.8 to 24.9 GPa and 500 to 1800°C, respectively.

[60] Temperature and pressure conditions in the Moon similar to those at Earth's brittle-ductile transition are reached near approximately 300 km depth in the lunar interior, so ductile flow should dominate in the active moonquake zone

Table 3. Percent of Hemispherical Surface Area Spanned by Grid Elements With Variance Ratios Less Than or Equal to 1.05 Times the Minimum Value[a]

Cluster	Equation 1	Equation 11	$\delta\pm$ (deg)	$\alpha\pm$ (deg)
A1	10.2	1.6		
A3	1.6	0.4	10	10
A6	3.4	0.3	10	10
A7	4.3	0.4	10	10
A8	0.9	5.8		
A9	0.3	2.4	10	20
A10	0.6	0.3	10	10
A13	0.4	0.3	10	10
A14[b]	2.1	2.1		
A15	12.9	0.5	10	10
A16[b]	0.5	0.5		
A17	0.4	1.9	10	10
A18[b]	0.4	0.4		
A19	2.1	0.4	10	10
A20	4.6	0.8	10	30
A21[b]	0.3	0.3		
A22	0.5	1.4	10	10
A25[b]	0.5	0.5		
A26	0.1	2.8	10	30
A30	0.5	0.3	10	10
A32	1.2	0.3	10	10
A33	0.7	0.1	10	10
A34[b]	0.3	0.3		
A36	4.6	1.0		
A37	2.6	1.0		
A38	1.1	0.8		
A40[b]	0.3	0.3		
A41[b]	0.3	0.3		
A42	2.0	0.3	10	10
A44	0.3	0.4		
A51[b]	0.4	0.4		
A65	0.9	0.3	10	10
A73	0.2	0.3	10	10
A96	0.5	0.1	10	10
A97	1.1	0.4	10	10
A202	0.1	0.5	10	20
A234[b]	0.5	0.5		
A238	1.9	1.0		
A257	1.1	0.5	10	10

[a]Boldface type indicates clusters for which all grid elements corresponding less than or equal to 1.05 times the minimum variance ratio reside in a single local minimum. The resulting fault plane orientation uncertainties are listed in the rightmost columns.

[b]The 1.05 measure was equal for both failure criteria.

(between 600 and 1000 km depth), where the pressures and temperatures range from 3.2 to 3.9 GPa and 1000 to 1500°C, respectively [*Hood and Zuber*, 2000; *Lognonné et al.*, 2003; *Gagnepain-Beyneix et al.*, 2006]. Yet for both deep moonquakes and deep earthquakes, we know from observations of seismograms that despite the conditions in the deep interior of both bodies, shear failure is still occurring there.

[61] One mechanism that is widely accepted for deep earthquakes and has recently been suggested for deep moonquakes [*Frohlich and Nakamura*, 2007] is "dehydration embrittlement," which requires the presence of hydrous minerals at the depth of failure [*Frohlich*, 2006]. Although recent works pronounce the Moon to be "wetter" than was previously accepted [*McCubbin et al.*, 2007; *Saal et al.*, 2008], volatile content is still estimated to be extremely low.

[62] Another hypothesis that has been proposed for the occurrence of deep earthquakes is "transformational faulting," in which shear failure is induced by mineral phase changes in the Earth's interior [*Frohlich*, 2006]. In response to an applied stress, a mineral with two stable forms can change from its low-pressure form to its high-pressure form. One such phase change in the Earth is the olivine-spinel transformation. Laboratory experiments designed to reproduce this transformation [*Green and Burnley*, 1989] show that in certain temperature/pressure environments consistent with deep earthquakes, the phase change initiates as lens-shaped "anticracks" of spinel, which produce stress concentrations at their tips. As anticracks form, they release heat, which increases their rate of formation. As the anticracks grow and their numbers increase, they link and eventually reach a critical density. When this occurs, the material can no longer support the applied stress, and catastrophic shear failure occurs along the growing anticrack instability.

[63] If (1) there is an appropriate phase transition in the lunar interior (pressures in the Moon are too low for the olivine-spinel transformation) and (2) this phase change could happen repeatedly and reversibly in response to the periodic tidal forcing, this mechanism may explain the following observations at those clusters for which our grid search method does not produce a clear best fitting plane:

[64] 1. For some clusters, the best fitting stress state does not depend strongly on plane orientation. This suggests that failure is occurring in a distinct volume, rather than along a preexisting plane.

[65] 2. Some clusters have best fitting linear combinations of shear and normal stress for which the relative contribution of normal stress is larger. This may be indicative of transformational faulting in which anticracks are observed to form perpendicular to the maximum compressive stress.

[66] 3. Some clusters have best fitting linear combinations of stresses and stress rates for which the plane orientation is better constrained than that associated with the linear combination of just stresses. It is plausible that there be a delay between the stress state that marks the onset of anticrack formation and the eventual coalescence of anticracks that leads to failure, so transformational faulting could also describe our observation that moonquakes respond significantly to stress rates.

6. Conclusions

[67] Deep moonquakes provide a unique opportunity to analyze the present conditions of the dynamic lunar interior. We have determined that failure on a plane due to elastic stresses and stress rates cannot explain the temporal occurrence of deep moonquakes at many clusters. Importantly, the timing of events at those clusters that were the most seismically active over the course of the Apollo experiment cannot be explained by such a model. However, deep moonquake occurrence at 13 out of 39 (33%) clusters can be explained by linear combinations of normal and shear tidal stresses (and/or stress rates), as resolved onto failure planes such that the stress combinations are approximately constant at moonquake times. Failure at each cluster is locally determined, with failure planes at individual clusters having different orientations, even for nearby clusters. Several of our results support the hypothesis of transformational faulting as a plausible failure mechanism. Future work is needed to identify whether candidate phase changes exist, and to better un-

derstand the rheological properties of the Moon, at deep moonquake depths.

Appendix A: Tidal Stress Formulation

[68] The response of the Moon to the tidal influence of the Earth is linear, so for the degree 2 spherical harmonic term in the Earth's gravitational potential, there is a corresponding degree 2 deformation pattern on the Moon. In order to determine that pattern, we need to construct and solve a set of differential equations which govern the elastic gravitational response of an initially spherical body. The standard approach is to expand the displacement vector, stress tensor, and gravitational potential perturbation in spherical harmonics, and determine the relationship between the corresponding radial factors. We now briefly summarize that process.

[69] The values of the displacements $\mathbf{u} = (u_r, u_\theta, u_\phi)$ are proportional to the imposed potential and can be expressed as products of two terms: a radially varying term y_i, and an angular term that can be expanded with Legendre polynomials:

$$u_r = \sum_{n=1}^{\infty} y_1(n,r) P_n(\cos\Delta) \tag{A1}$$

$$u_\theta = \sum_{n=1}^{\infty} y_2(n,r) \partial_\theta P_n(\cos\Delta) \tag{A2}$$

$$u_\phi = \sum_{n=1}^{\infty} \frac{y_2(n,r)}{\sin\theta} \partial_\phi P_n(\cos\Delta) \tag{A3}$$

Note that the two nonradial components of the displacement vector, u_θ and u_ϕ, share a single radial factor, y_2.

[70] The elastic strain tensor is obtained via the gradient of the displacement vector. The components of the stress tensor that are strictly nonradial can be determined from the corresponding strain tensor components; those stress terms with a radial component (σ_{rr}, $\sigma_{r\theta}$, $\sigma_{r\phi}$) have both elastic and gravitational contributions. Their spatial variations can be expressed in a form which parallels that used for the displacement vector:

$$\sigma_{rr} = \sum_{n=1}^{\infty} y_3(n,r) P_n(\cos\Delta) \tag{A4}$$

$$\sigma_{r\theta} = \sum_{n=1}^{\infty} y_4(n,r) \partial_\theta P_n(\cos\Delta) \tag{A5}$$

$$\sigma_{r\phi} = \sum_{n=1}^{\infty} \frac{y_4(n,r)}{\sin\theta} \partial_\phi P_n(\cos\Delta) \tag{A6}$$

where $y_3(n, r)$ and $y_4(n, r)$ are the corresponding radial factors for stress.

[71] The perturbation to the Moon's gravitational potential due to these deformations can be similarly expressed:

$$\phi_1 = \sum_{n=1}^{\infty} y_5(n,r) P_n(\cos\theta) \tag{A7}$$

It must satisfy Poisson's equation:

$$\nabla^2 \phi_1 = 4\pi G \rho_1 \tag{A8}$$

which is a second-order differential equation. Any such second-order equation can be rewritten as a set of coupled first-order equations.

[72] Following the formulation of *Alterman et al.* [1959], the six radially varying functions $y_i(n, r)$ describe the elastic gravitational deformation of a body in response to seismically induced (e.g., Earth's normal modes) or tidally induced (as we consider) deformations. Since we are only interested in degree $n = 2$, we will subsequently drop the n dependence of the y_i's. The radial factors are: y_1, the radial factor of the radial component of displacement (u_r), y_2, the radial factor of the tangential components of displacement (u_θ and u_ϕ), y_3, the radial factor of the radial component of stress (σ_{rr}), y_4, the radial factor of the tangential components of stress ($\sigma_{r\theta}$ and $\sigma_{r\phi}$), y_5, the radial factor of the potential, and y_6, the radial factor of the "potential stress," defined such that the gradient of the potential is continuous across the surface of the Moon.

[73] We consider the incompressible case, for which the differential equations for the y_i's can be written in matrix form [*Wu and Peltier*, 1982]:

$$\frac{d\mathbf{y}}{dr} = \mathbf{A} \cdot \mathbf{y} \tag{A9}$$

where $\mathbf{A}$ is a matrix consisting of coefficients from the equations of motion and $\mathbf{y}(r)$ is the solution vector (y_1, y_2, y_3, y_4, y_5, y_6).

[74] The solutions to this system of equations are subject to the following boundary conditions for a homogeneous Moon: (1) the surface of the Moon is stress-free, (2) the gravitational potential is continuous across the surface of the Moon, and (3) the displacement and potential are regular at the center of the Moon.

[75] The solution vector $\mathbf{y}$ can be represented generally as a linear combination of six independent solutions $\mathbf{y} = \mathbf{Y} \cdot \mathbf{c}$, where $\mathbf{Y}$ is called the fundamental matrix and $\mathbf{c}$ is a 6-component vector of coefficients [*Sabadini and Vermeersen*, 2004]. The fundamental matrix $\mathbf{Y}$ consists of two parts such that $\mathbf{Y} = [\mathbf{Y}_1 \mathbf{Y}_2]$. In this formulation, $\mathbf{Y}_1$ is the set of three regular solution vectors (positive powers of r):

$$\mathbf{Y}_1 = \begin{bmatrix} n r^{1+n} & n r^{-1+n} & 0 \\ \frac{(3+n) r^{1+n}}{1+n} & r^{-1+n} & 0 \\ r^n \left(2\left(-3+(n-1)n\right)\mu + g n r \rho\right) & n r^{-2+n} \left(2(n-1)\mu + g r \rho\right) & r^n \rho \\ \frac{2n(2+n) r^n \mu}{1+n} & 2(n-1) r^{-2+n} \mu & 0 \\ 0 & 0 & r^n \\ 4 G n \pi r^{1+n} \rho & 4 G n \pi r^{-1+n} \rho & (1+2n) r^{-1+n} \end{bmatrix} \tag{A10}$$

where g, ρ, and μ are the gravity, density, and rigidity of the Moon model and $n = 2$ for tides. The corresponding irregular solution vectors (negative powers of r) are in $\mathbf{Y}_2$:

$$\mathbf{Y}_2 = \begin{bmatrix} n(1+n)r^{-n} & (1+n)r^{-2-n} & 0 \\ (2-n)r^{-n} & -r^{-2-n} & 0 \\ n r^{-1-n}\left(-2\left(-1+n(3+n)\right)\mu + g(1+n)r\rho\right) & (1+n)r^{-3-n}\left(-2(2+n)\mu + g r\rho\right) & r^{-1-n}\rho \\ 2\left(-1+n^2\right)r^{-1-n}\mu & 2(2+n)r^{-3-n}\mu & 0 \\ 0 & 0 & r^{-1-n} \\ 4Gn(1+n)\pi\rho r^{-n} & 4G(1+n)\pi r^{-2-n}\rho & 0 \end{bmatrix} \quad \text{(A11)}$$

Each column of the fundamental matrix represents an independent solution of equation (A9). The coefficients c_i are determined by the boundary conditions, now expressed as (1) $y_3(R) = y_4(R) = 0$ where R is the radius of the Moon, (2) $y_6(R) = -\frac{(2n+1)}{R}$, and (3) $y_1(0) = y_2(0) = y_5(0) = 0$. The requirement that the solutions be regular at the origin reduces the number of independent solutions from six to three, since $\mathbf{Y}_2$ is undefined at the origin. The three coefficients are determined by forming the linear combination of solution vectors that satisfies the remaining boundary conditions $(y_3(R), y_4(R), y_6(R)) = (0, 0, -\frac{(2n+1)}{R}) = \mathbf{b}$.

[76] This is accomplished using the projection matrix

$$\mathbf{P} = \begin{bmatrix} 0 & 0 & 0 \\ 0 & 0 & 0 \\ 1 & 0 & 0 \\ 0 & 1 & 0 \\ 0 & 0 & 0 \\ 0 & 0 & 1 \end{bmatrix} \quad \text{(A12)}$$

The projection matrix selects out the y_3, y_4, and y_6 terms from each regular solution vector, which must satisfy the boundary conditions at the surface, discussed above. The three coefficients necessary to compute the correct linear combination of the regular solution vectors can be found from:

$$\mathbf{c} = \left(\mathbf{P}^T \cdot \mathbf{Y}\right)^{-1}\mathbf{b} \quad \text{(A13)}$$

Once the correct linear combination of regular solutions $\mathbf{y} = \mathbf{Y}_1 \cdot \mathbf{c}$ has been obtained, the desired harmonic degree ($n = 2$ for tides) can be substituted into $\mathbf{Y}_1$ to obtain the solution 6-vector $\mathbf{y}(r)$ in terms of the density, rigidity, gravitational constant, outer radius of the Moon, and desired inner radius at which the stress is to be computed. Of these, y_1 through y_4 are used in our formulation of the stress tensor.

[77] In the next step, we include the time-varying gravitational tidal potential when computing the vector displacement. As discussed earlier, the components of the displacement vector $\mathbf{u} = (u_r, u_\theta, u_\phi)$ are products of radial and angular terms, with (r_s, θ_s, ϕ_s) describing the time-varying position of the Earth, and (r, θ, ϕ) describing the position within the Moon at which stresses are computed.

[78] The elastic strain tensor ϵ_{ij} is formed by taking the vector gradient of the tidal displacement ($\nabla\mathbf{u}$) and symmetrizing the resulting tensor.

$$\nabla\mathbf{u} = \begin{bmatrix} \frac{\partial u_r}{\partial r} & \frac{1}{r}\left(\frac{\partial u_r}{\partial\theta} - u_\theta\right) & \frac{1}{r\sin\theta}\left(\frac{\partial u_r}{\partial\phi} - u_\phi\sin\theta\right) \\ \frac{\partial u_\theta}{\partial r} & \frac{1}{r}\left(\frac{\partial u_\theta}{\partial\theta} + u_r\right) & \frac{1}{r\sin\theta}\left(\frac{\partial u_\theta}{\partial\phi} - u_\phi\cos\theta\right) \\ \frac{\partial u_\phi}{\partial r} & \frac{1}{r}\frac{\partial u_\phi}{\partial\theta} & \frac{1}{r\sin\theta}\frac{\partial u_\phi}{\partial\phi} + \frac{u_r}{r} + \frac{u_\theta\cot\theta}{r} \end{bmatrix} \quad \text{(A14)}$$

$$\epsilon_{ij} = \frac{\nabla\mathbf{u} + (\nabla\mathbf{u})^T}{2} \quad \text{(A15)}$$

Tangential stresses ($\sigma_{\theta\theta}$, $\sigma_{\theta\phi}$, and $\sigma_{\phi\phi}$) are related to tangential strains through equation (5). The elastic strain tensor ϵ_{ij}, however, does not account for the effect of self-gravitation, which affects all radial components of stress (σ_r, $\sigma_{r\theta}$, and $\sigma_{r\phi}$). In the same manner in which we computed the displacement vector terms, the radial components of stress are products of radial and angular terms. Time variation is introduced to the stress tensor σ_{ij} through the changing coordinates (distance r_s, colatitude θ_s, and longitude ϕ_s) of the tide-raising source body (the Earth) as computed from MICA, the MultiYear Interactive Computer Almanac [*United States Naval Observatory*, 2004].

[79] Since each element in the stress tensor can be written as a product of terms dependent on source coordinates (r_s, θ_s, ϕ_s) and position within the Moon (r, θ, ϕ), the phase of the temporal variation of the tidal stress (i.e., the timing of stress peaks) is independent of the internal structure model [*Minshull and Goulty*, 1988]. This means that any investigation of the relationship between tidal stress and moonquake occurrence times does not require a precise knowledge of the lunar interior. The variation of density and elastic moduli with radius affects only the magnitude of the elements of the stress tensor at a given depth. Therefore in our calculations, we use a homogeneous model of the lunar interior, with density $\rho = 3000$ kg/m^3 and rigidity $\mu = 10^{10}$ Pa.

[80] **Acknowledgments.** The authors would like to thank Justin Hagerty, Robin Fergason, Yosio Nakamura, Cliff Frohlich, and an anonymous reviewer for their thoughtful comments on this manuscript. This work was supported by the Eugene M. Shoemaker Planetary Geology and Geophysics Fellowship awarded to R.C.W., and grants NASA-NNG05GK34G, NASA-NNX08AL49G, and NSERC to C.L.J.

References

Aki, K., and P. G. Richards (2002), *Quantitative Seismology*, 2nd ed., Univ. Sci. Books, Sausalito, Calif.

Alterman, Z., H. Jarosch, and C. L. Pekeris (1959), Oscillations of the Earth, *Proc. R. Soc. London*, *252*(1268), 80–95.

Araki, H. (2001), Focal processes of deep moonquakes, *J. Geod. Soc. Jpn.*, *47*(1), 508–513.

Bills, B. G., R. Bulow, and C. L. Johnson (2008), Influence of Earth-Moon orbit geometry on deep moonquake occurrence times, *Lunar Planet. Sci.*, *XXXIX*, Abstract 1735.

Bott, M. H. P. (1982), *The Interior of the Earth: Its Structure, Constitution, and Evolution*, Elsevier, New York.

Bulow, R. C. (2007), New events from the Apollo lunar seismic data and an investigation of the relationship between tidal stress and deep moonquake occurrence, Ph.D. thesis, Univ. of Calif., San Diego, La Jolla.

Bulow, R. C., C. L. Johnson, and P. M. Shearer (2005), New events discovered in the Apollo lunar seismic data, *J. Geophys. Res.*, *110*, E10003, doi:10.1029/2005JE002414.

Bulow, R. C., C. L. Johnson, B. G. Bills, and P. M. Shearer (2007), Temporal and spatial properties of some deep moonquake clusters, *J. Geophys. Res.*, *112*, E09003, doi:10.1029/2006JE002847.

Cheng, C. H., and M. N. Toksöz (1978), Tidal stresses in the Moon, *J. Geophys. Res.*, *83*, 845–853.

Evans, B., J. T. Fredrich, and T. Wong (1990), The brittle-ductile transition in rocks: Recent experimental and theoretical progress, in *The Brittle-Ductile Transition in Rocks: The Heard Volume*, *Geophys. Monogr. Ser.*, vol. 56, edited by A. G. Duba et al., pp. 1–20, AGU, Washington D. C.

Ewing, M., G. Latham, F. Press, G. Sutton, J. Dorman, Y. Nakamura, R. Meissner, F. Duennebier, and R. Kovach (1971), Seismology of the Moon and implications on internal structure, origin and evolution, in *Highlights of Astronomy*, pp. 155–172, D. Reidel, Dordrecht, Netherlands.

Frohlich, C. (1989), The nature of deep-focus earthquakes, *Annu. Rev. Earth Planet. Sci.*, *17*, 227–254.

Frohlich, C. (2006), *Deep Earthquakes*, Cambridge Univ. Press, Cambridge, U. K.

Frohlich, C., and Y. Nakamura (2007), Geographic variations in the tidal control of deep moonquake nests and speculation about their mechanical origin, *Lunar Planet. Sci.*, *XXXVIII*, Abstract 1749.

Gagnepain-Beyneix, J., P. Lognonné, H. Chenet, D. Lombardi, and T. Spohn (2006), A seismic model of the lunar mantle and constraints on temperature and mineralogy, *Phys. Earth Planet. Inter.*, *159*, 140–166.

Goins, N. R., A. M. Dainty, and M. N. Toksöz (1981), Seismic energy release of the Moon, *J. Geophys. Res.*, *86*, 378–388.

Goulty, N. R. (1979), Tidal triggering of deep moonquakes, *Phys. Earth Planet. Inter.*, *19*, 52–58.

Green, H. W., and P. C. Burnley (1989), A new self-organizing mechanism for deep-focus earthquakes, *Nature*, *341*, 733–737.

Hood, L. L., and M. T. Zuber (2000), Recent refinements in geophysical constraints on lunar origin and evolution, in *Origin of the Earth and Moon*, pp. 397–409, Univ. of Ariz. Press, Tucson.

Koyama, J., and Y. Nakamura (1980), Focal mechanism of deep moonquakes, *Proc. Lunar Planet. Sci. Conf., 11th*, *3*, 1855–1865.

Lammlein, D. R. (1977), Lunar seismicity and tectonics, *Phys. Earth Planet. Inter.*, *14*, 224–273.

Lammlein, D. R., G. V. Latham, J. Dorman, Y. Nakamura, and M. Ewing (1974), Lunar seismicity, structure, and tectonics, *Rev. Geophys.*, *12*(1), 1–21.

Latham, G., M. Ewing, F. Press, and G. Sutton (1969), The Apollo passive seismic experiment, *Science*, *165*, 241–250.

Latham, G., M. Ewing, J. Dorman, D. Lammlein, F. Press, N. Toksoz, G. Sutton, F. Duennebier, and Y. Nakamura (1971), Moonquakes, *Science*, *174*, 687–692.

Lognonné, P., G. Gagnepain-Beyneix, and H. Chenet (2003), A new seismic model of the moon: Implications for structure, thermal evolution and formation of the moon, *Earth Planet. Sci. Lett.*, *211*, 27–44.

Love, A. E. H. (1967), *Some Problems of Geodynamics: Being an Essay to Which the Adams Prize in the University of Cambridge was Adjudged in 1911*, Dover, New York.

McCubbin, F. M., H. Nekvasil, and D. H. Lindsley (2007), Is there evidence for water in lunar magmatic minerals? A crystal chemical investigation, *Lunar Planet. Sci.*, *XXXVIII*, Abstract 1354.

Meissner, R. (1977), Lunar viscosity models, *Philos. Trans. R. Soc. London., Ser. A*, *285*(1327), 463–467.

Minshull, T. A., and N. R. Goulty (1988), The influence of tidal stresses on deep moonquake activity, *Phys. Earth Planet. Inter.*, *52*, 41–55.

Nakamura, Y. (1978), A1 moonquakes: Source distribution and mechanism, *Proc. Lunar Planet. Sci. Conf., 9th*, *3*, 3589–3607.

Nakamura, Y. (2003), New identification of deep moonquakes in the Apollo lunar seismic data, *Phys. Earth Planet. Inter.*, *139*, 197–205.

Nakamura, Y. (2005), Farside deep moonquakes and deep interior of the moon, *J. Geophys. Res.*, *110*, E01001, doi:10.1029/2004JE002332.

Nakamura, Y. (2007), Within-nest hypocenter distribution and waveform polarization of deep moonquakes and their possible implications, *Lunar Planet. Sci.*, *XXXVIII*, Abstract 1160.

Nakamura, Y., G. V. Latham, H. J. Dorman, and J. E. Harris (1981), Passive seismic experiment long period event catalog, revised July 2004, *Tech. Rep. 118*, Inst. for Geophys., Univ. of Tex. Austin.

Pollard, D. D., and R. C. Fletcher (2005), *Fundamentals of Structural Geology*, Cambridge Univ. Press, Cambridge, U. K.

Saal, A. E., E. H. Hauri, M. L. Cascio, J. A. Van Orman, M. C. Rutherford, and R. F. Cooper (2008), Volatile content of lunar volcanic glasses and the presence of water in the Moon's interior, *Nature*, *454*, 192–195.

Sabadini, R., and B. Vermeersen (2004), Normal mode theory in viscoelasticity, in *Global Dynamics of the Earth: Applications of Normal Mode Relaxation Theory to Solid-Earth Geophysics*, pp. 1–44, Kluwer Acad., Dordrecht, Netherlands.

Smith, B., and D. Sandwell (2003), Coulomb stress accumulation along the San Andreas fault system, *J. Geophys. Res.*, *108*(B6), 2296, doi:10.1029/2002JB002136.

Stacey, F. D. (1992), *Physics of the Earth*, Brookfield Press, Brisbane, Queensl., Australia.

Stegman, D. R., A. M. Jellinek, S. A. Zatman, J. R. Baumgardner, and M. A. Richards (2003), An early lunar core dynamo driven by thermochemical mantle convection, *Nature*, *421*, 143–146.

Toksöz, M. N., N. R. Goins, and C. H. Cheng (1977), Moonquakes: Mechanisms and relation to tidal stresses, *Science*, *196*, 979–981.

United States Naval Observatory (2004), *United States Naval Observatory Multi-Year Interactive Computer Almanac* [CD-ROM], Willmann-Bell, Richmond, Va.

Wu, P., and W. R. Peltier (1982), Viscous gravitational relaxation, *Geophys. J. R. Astron. Soc.*, *70*(2), 435–485.

B. G. Bills and C. L. Johnson, Cecil H. and Ida M. Green Institute of Geophysics and Planetary Physics, Scripps Institution of Oceanography, University of California, San Diego, La Jolla, CA 92093, USA.

R. C. Weber, U.S. Geological Survey, 2255 North Gemini Drive, Flagstaff, AZ 86001, USA. (rweber@usgs.gov)